MOLECULAR IMAGING AND BIOLOGY

Mol Imaging Biol (2017)
DOI: 10.1007/s11307-017-1108-4

RESEARCH ARTICLE

PET Imaging on Dynamic Metabolic Changes after Combination Therapy of Paclitaxel and the Traditional Chinese Medicine in Breast Cancer-Bearing Mice

Yao Chen,[1,2,3,4] Ling Wang,[1,2,3,4] Hao Liu,[1,2,3,4] Fahuan Song,[1,2,3,4] Caiyun Xu,[1,2,3,4] Kai Zhang,[1,2,3,4] Qing Chen,[1,2,3,4] Shuang Wu,[1,2,3,4] Yunqi Zhu,[1,2,3,4] Ying Dong,[5] Min Zhou,[1,2,3,4,6] Hong Zhang,[1,2,3,4] Mei Tian[1,2,3,4]

[1]*Department of Nuclear Medicine, The Second Hospital of Zhejiang University School of Medicine, 88 Jiefang Road, Hangzhou, Zhejiang, 310009, China*
[2]*Zhejiang University Medical PET Center, Zhejiang University, Hangzhou, China*
[3]*Institute of Nuclear Medicine and Molecular Imaging, Zhejiang University, Hangzhou, China*
[4]*Key Laboratory of Medical Molecular Imaging of Zhejiang Province, Hangzhou, China*
[5]*Department of Oncology, The Second Hospital of Zhejiang University School of Medicine, Hangzhou, China*
[6]*Institute of Translational Medicine, Zhejiang University, Hangzhou, China*

Abstract

Purpose: The aim of the study was to non-invasively evaluate the anticancer activity of a traditional Chinese medicine—Huaier, combined with paclitaxel (PTX) in breast cancer bearing mice by detecting dynamic metabolic changes with positron emission tomography (PET).

Procedures: Balb/c nude mice were randomly divided into one of the four groups: Huaier, PTX, PTX + Huaier, or the control. PET imaging with 2-deoxy-2-[^{18}F]fluoro-D-glucose ([^{18}F]FDG) was performed to monitor the metabolic changes in BT474 (luminal B) and MDA-MB-231 (triple-negative) breast cancer xenografts. Immunohistochemistry (IHC) study was performed immediately after the final PET scan to assess the expressions of phosphatidylinositol 3-kinase (PI3K), phospho-AKT (p-AKT), caspase-3, and vascular endothelial growth factor (VEGF).

Results: Compared to the control group, [^{18}F]FDG accumulation demonstrated a significant decrease in PTX + Huaier ($p < 0.01$) or Huaier group ($p < 0.05$), which was consistent to the decreased expression of PI3K ($p < 0.05$) and p-AKT ($p < 0.05$) in the breast cancer xenografts.

Conclusion: The therapeutic effect of Huaier combined with PTX was superior than the PTX alone in BT474 and MDA-MB-231 breast cancer-bearing mice. [^{18}F]FDG PET imaging could be a potential non-invasive approach to assess the metabolic changes after chemotherapy combined with traditional Chinese medicine in the breast cancer.

Key words: Positron emission tomography (PET), Traditional Chinese medicine (TCM), Paclitaxel, Breast cancer

Yao Chen and Ling Wang contributed equally to this work.

Correspondence to: Mei Tian; *e-mail:* meitian@zju.edu.cn

Published online: 09 August 2017

Introduction

Breast cancer is one of the leading causes of cancer deaths in women [1]. In each year, nearly 1.7 million women are diagnosed with breast cancer worldwide, and approximately 500,000 die from this disease [2]. Breast cancer is a heterogeneous disease, four common subtypes have been identified (luminal A, luminal B, triple-negative, and HER2 overexpression type). Currently, available therapies are chemotherapy [3], endocrine therapy [4], human epidermal growth factor receptor 2 (HER2)-targeted therapy [5], surgery [6], and radiotherapy [7]. Despite these treatment options, limited success has been made in terms of treatment outcomes. Therefore, alternative or complimentary medicine is warranted in the clinical patient management. Recently, western therapeutic drugs combined with traditional Chinese medicine (TCM) have been found to have significantly improved the therapeutic effect in hepatocellular [8], ovarian [9], gastric [10], and breast cancers [11]. In particular, Trametes Robiniophila Murr (Huaier), a sandy beige mushroom on the hardwood tree trunks [12], has been used as a traditional herbal medicine for about 1600 years in China. The effective ingredient of Huaier extract is proteoglycan, which contains 41.53 % of polysaccharides, 12.93 % of amino acids, and 8.72 % of water [12]. It has been reported that Huaier can not only enhance the immune response [13] but also induce the anti-tumor effect [14]. Paclitaxel (PTX), a classical anticancer drug, has been used clinically for decades [15]. Very recently, PTX combined with Huaier has been used as an alternative option for breast cancer patients [16]. However, to date, we have limited understanding on the therapeutic mechanisms of Huaier, and no biomarker has been established for its outcomes.

Malignant tumor cells utilize glucose to produce lactic acid even under non-hypoxic conditions, which is known as Warburg effect [17]. It is associated with the high rate of glucose metabolism of cancer cells which often occurs in breast cancer in parallel with a marked increase of glucose uptake and consumption [18]. Since the increased glucose metabolism can be visualized by 2-deoxy-2-[^{18}F]fluoro-D-glucose ([^{18}F]FDG) positron emission tomography (PET), we hypothesized that [^{18}F]FDG PET could be used as a representative molecular imaging technology to measure glucose metabolic changes after PTX is combined with Huaier in breast cancer-bearing animals [19–21].

In this study, we performed [^{18}F]FDG PET imaging on a weekly basis to non-invasively evaluate the glucose metabolic changes after Huaier alone and combined therapy of Huaier + PTX in breast cancer-bearing mice and to evaluate the expressions of phosphatidylinositol 3-kinase (PI3K), phospho-AKT (p-AKT), caspase-3, and vascular endothelial growth factor (VEGF).

Materials and Methods

Cell Culture and Reagents

Human breast cancer cell lines BT474 (luminal B) and MDA-MB-231 (triple-negative) were purchased from Shanghai Institute of Cell Biology of the Chinese Academy of Sciences. BT474 and MDA-MB-231 cells were cultured in RPMI-1640 medium (Gibco, USA) and Dulbecco's modified Eagle's medium (Gibco), respectively. The medium was supplemented with 10 % heat-inactivated fetal bovine serum (HyClone, USA), 100 U/ml penicillin, and 100 μg/ml streptomycin under the conditions of 5 % CO_2 at 37 °C.

Electuary ointment of Huaier was donated by Gaitianli Medicine Co. Ltd. (Gaitianli, China). The electuary ointment (2 g) was dissolved in 20 ml of complete medium. The solid residue of the above dissolved ingredient was filtered and discarded through a 0.22-μm filter. The final 100 mg/ml stock solution was kept at −20 °C for long storage [22, 23]. PTX (Taxol®, H20130359) was obtained from Bristol-Myers Squibb S.R.L (Bristol-Myers Squibb, Italy).

Cell Viability Assay

Cell viability was determined by Cell Counting Kit-8 (CCK-8, Dojindo, Japan) assay. BT474 (1×10^4 cells/well) and MDA-MB-231 (3×10^3 cells/well) cells were seeded in 96-well plates. After incubation overnight, the medium in each well was replaced with Huaier (0, 2, 4, 8, and 16 mg/ml) [12], PTX (0, 0.1, 1, 10, and 100 μg/ml) [24], and drug combination (PTX of 0.1 μg/ml combined with five different concentrations of Huaier). Subsequently, cells were incubated for 48 h, individually. Afterwards, all the solutions were removed and 100 μl medium with 10 μl CCK-8 were added to each well. Then, the cells were incubated for another 4 h at 37 °C. Absorbance values were finally measured by the Microplate Reader (Bio-Rad, USA) at 450 nm.

Animal Experiments

Breast cancer cells (2×10^7 of BT474 or 3×10^6 of MDA-MB-231) were injected subcutaneously into the right flank of female Balb/c nude mice (Zhejiang Academy of Medical Sciences, China). All the mice were randomly divided into the control, Huaier, PTX or PTX + Huaier group ($n = 5$ for each group) when tumors reached to 5 mm in diameter. The control group was given 100 μl saline daily by gavage; the Huaier group was treated with a 100-μl solution containing saline and 50 mg Huaier extract by gavage once a day; the mice in the PTX group were given intraperitoneally with a 100-μl solution containing saline and PTX (10 mg/kg) once a week; and the mice in the PTX + Huaier treatment group were given the combined treatment of PTX and Huaier. Tumor size was measured twice a week and calculated using the following formula: Volume = length × width × width × 0.5. A tumor growth index (TGI) was calculated according to the following formula: $TGI = (Vol_{t=X} - Vol_{t=0})/Vol_{t=0}$.

All animal experiments were carried out in accordance with the National Institutes of Health Guide for the Care and

Use of Laboratory Animals and approved by the Institutional Animal Care and Use Committee of Zhejiang University (Protocol No. ZJU201407-1-01-071).

[^{18}F]FDG Small Animal PET Imaging and Image Analysis

All mice underwent [^{18}F]FDG small animal PET on days 0 (before treatment), 7, 14, and 21. After injection with approximately 7.4 MBq (200 μCi) of [^{18}F]FDG *via* the tail vein, the mice were maintained anesthetized with 1.5 % isoflurane. At 60 min post-injection, the mice were scanned using an acquisition time of 10 min by a small animal PET R4 scanner (Concorde Microsystems, USA). [^{18}F]FDG accumulation was calculated as the percentage of injected dose per gram (%ID/g) of tissue using the ASIPro software (Concorde Microsystems). Tumor-to-homologous contralateral muscle (T/M) ratio was used for semi-quantitative analysis, calculated by the following formula: T/M ratio = max counts per pixel of tumor region of interest/max counts per pixel of homologous contralateral muscle area. Then, the change in T/M ratio was calculated with the use of the following formula: change in T/M ratio on Day N = (T/M ratio on Day N − T/M ratio on Day 0) / T/M ratio on Day 0 × 100 % (N = 7, 14, and 21).

Immunohistochemistry (IHC) Staining

Following the final PET acquisition, mice were sacrificed by cervical dislocation. The tumor tissues were collected for IHC study [25, 26]. Tumors were removed, dissected, and immersed in 4 % chilled paraformaldehyde in PBS (pH 7.4) for 24 h. After the tissue was paraffin embedded, 4-μm sections were processed with a sliding microtome (Microm, Germany). The specimens were stained with GTVision™ two-step strategy (Dako, Danmark). Afterward, the slides were incubated with 3 % hydrogen peroxide for 10 min and rinsed in PBS for about 5 min, then incubated overnight in a moist chamber at 4 °C with primary antibodies: rabbit polyclonal antibody against phosphatidylinositol 3-kinase (PI3K) (1:80 dilution; Cell Signaling Technology, USA); rabbit polyclonal antibody against phospho-AKT (p-AKT) (1:100 dilution; Santa Cruz Biotechnology, USA), rabbit polyclonal antibody against Caspase-3 (1:100 dilution; LabVision&NeoMarkers, USA), and rabbit polyclonal antibody against vascular endothelial growth factor (VEGF) (1:100 dilution; Santa Cruz Biotechnology). The sections were rinsed three times with PBS for 10 min and treated in horseradish peroxidase (HRP)-conjugated secondary antiserum for 30 min at 37 °C. Then, they were washed thoroughly and treated in diaminobenzidine (DAB) for 3–5 min until a brown reaction product was observed. To evaluate the integral optical density (IOD), they were achieved by averaging five microscopic fields (×200 magnification) using Image-ProPlus 6.0 software (Media Cybernetics, USA).

Statistical Analysis

Data were presented as mean ± SD. One-way ANOVA was used to assess TGI, T/M ratio change, and IOD between multiple groups. Correlation between TGI and T/M ratio change was determined using the Pearson correlation test. Statistical analyses were performed with SPSS software (version 19.0, SPSS Inc., USA). $p < 0.05$ was considered statistically significant.

Results

Cell Proliferation

To evaluate the effect of the Huaier extract on the BT474 and MDA-MB-231 cell lines, we measured cell viability using the CCK8 assay. Huaier and PTX significantly inhibited the growth of these two breast cell lines in a dose-dependent manner (Fig. 1). To determine the proper use of the PTX concentration, we tested the cell viability in BT474 and MDA-MB-231 cell lines (Fig. 1a). At the concentration of 0.1 μg/ml PTX treatment, no significant differences in the cell viabilities of these two cell lines were found compared with the control group (82.2 ± 9.2 and 81.5 ± 5.3 %, respectively, $p > 0.05$; Fig. 1a). However, at ≥1 μg/ml concentration, significant differences were demonstrated between the BT474/MDA-MB-231 group and the control group ($p < 0.05$; Fig. 1a). Based on these findings, 0.1 μg/ml PTX concentration was used in the subsequent combine therapy in both two cell lines. The BT474 cells (Fig. 1b) were more sensitive to the Huaier treatment, as the viability rates were decreased to 49.9 ± 7.0 % compared with 68.6 ± 11.2 % in the MDA-MB-231 cells at 8 mg/ml ($p < 0.05$). The cell viability in all combination groups was lower than that in the respective single-agent treatment groups. A significant decrease in cell viability was observed when the cells were treated with 4 mg/ml Huaier and 0.1 μg/ml PTX ($p < 0.05$).

Tumor Response

In the BT474-bearing xenografts, tumor growth was strongly inhibited by combined treatment of Huaier and PTX, but the changes of weight ratio in four groups had no significant difference. PTX + Huaier group demonstrated significantly lower TGI compared with the Huaier, PTX, and the control group as early as 7 days after treatment ($p < 0.05$; Fig. 2a). The single-treatment (Huaier alone or PTX alone) groups did not show a change in TGI compared to the control group. The weight of mice on day 7 to day 10 showed the tendency of decrease in the PTX + Huaier group to the control group; however, the changes of weight from days 14 to 21 had no

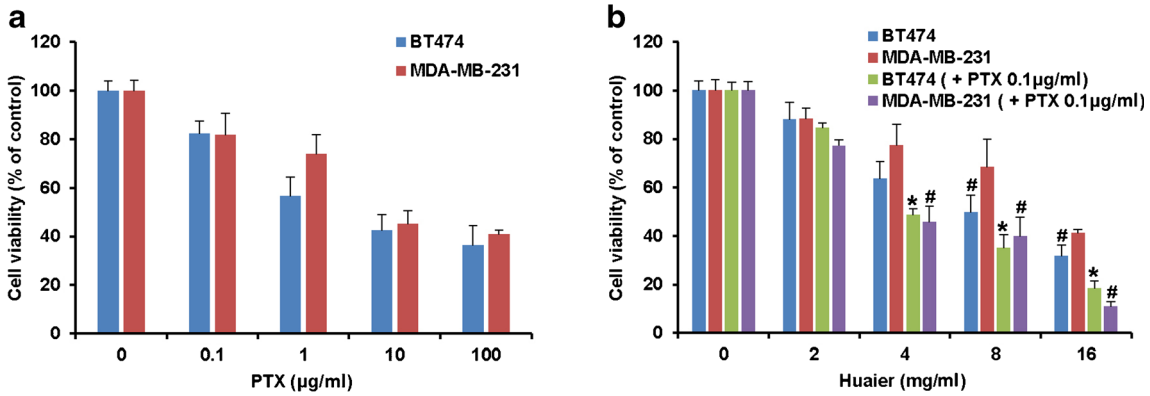

Fig. 1 Cell viability changes of BT474 and MDA-MB-231 cell lines after Huaier and/or PTX treatment. BT474 and MDA-MB-231 cells were treated respectively with **a** PTX (0.1, 1, 10, and 100 μg/ml) and **b** Huaier (2, 4, 8, and 16 mg/ml) with or without PTX (0.1 μg/ml) for 48 h. At the concentration of 0.1 μg/ml PTX treatment, no significant difference in the cell viabilities was found between either of these two cell lines and the control group (82.2 ± 9.2 and 81.5 ± 5.3 %, respectively, $p > 0.05$). The BT474 cells were more sensitive to the Huaier treatment, as the viability rate was decreased to 49.9 ± 7.0 % compared with 68.6 ± 11.2 % in the MDA-MB-231 cells at 8 mg/ml ($p < 0.05$). A significant decrease of cell viability was observed when 4 mg/ml of Huaier combined with 0.1 μg/ml of PTX in both BT474 ($p < 0.05$) and MDA-MB-231 ($p < 0.05$) cells, compared with the control.

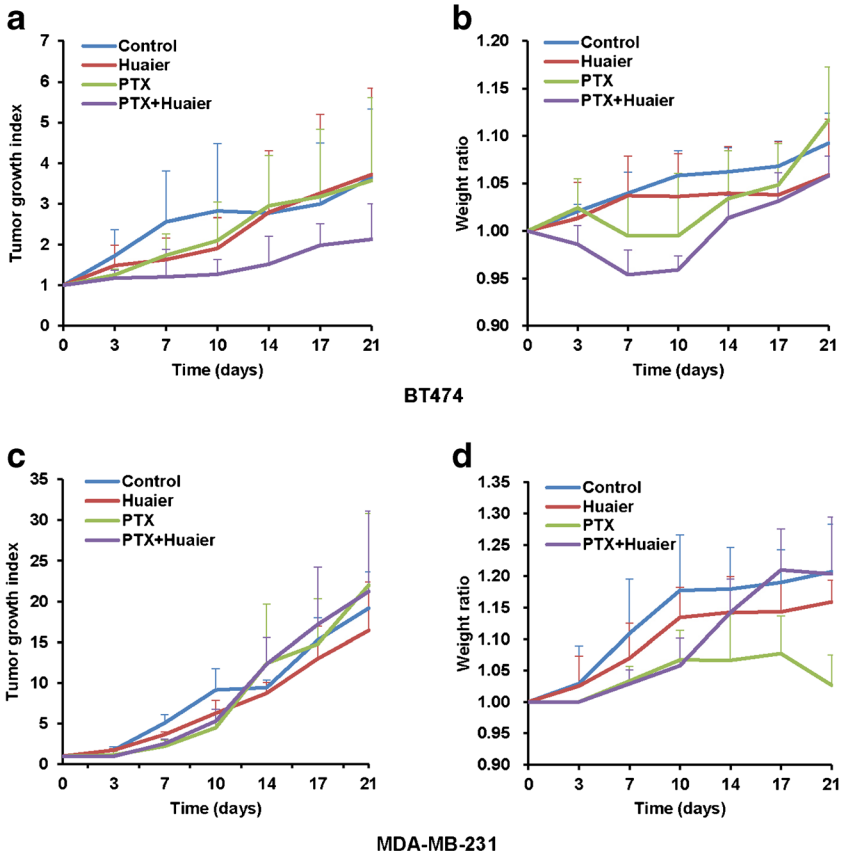

Fig. 2 The changes of **a** tumor growth index (TGI) and **b** body weight in mice bearing BT474 xenografts and **c** TGI and **d** body weight of mice bearing MDA-MB-231 xenografts. Mice were administered with saline, Huaier, PTX, and PTX + Huaier ($n = 5$ for each group), respectively. In BT474-bearing mice, the TGI of PTX + Huaier group was significantly lower than that of the Huaier, PTX, or control groups at 7 days after treatment ($p < 0.05$ for each comparison). In the MDA-MB-231-bearing mice, body weight loss in the PTX group was the most severe on day 21, compared with the other groups ($p < 0.05$ for each comparison).

significant difference for all the groups ($p > 0.05$; Fig. 2b). Nevertheless, with respect to MDA-MB-231 xenografts, the combination treatment did not show any significant inhibited effect compared to the other treatment strategies (Fig. 2c). Although there was no significant difference in TGI among all the therapies of MDA-MB-231 xenografts, the weight loss in the PTX group was the most severe among all the groups ($p < 0.05$; Fig. 2d).

Small Animal PET Imaging

With [^{18}F]FDG PET imaging, the visualization (Fig. 3a, b) and semi-quantification of glucose metabolism (Fig. 3c, d) of breast cancer xenografts were examined on days 0, 7, 14, and 21. There was no different in the tumor uptake of [^{18}F]FDG at 7 days in all the treated and control groups for both the BT474 and MDA-MB-231 xenografts ($p > 0.05$; Fig. 3c, d). After 14 days of PTX + Huaier therapy, however, there was a significant decrease in the uptake of [^{18}F]FDG in PTX + Huaier-treated mice, compared with the control mice bearing BT474 xenografts ($p < 0.05$; Fig. 3c). Furthermore, on day 14, tumor uptake of [^{18}F]FDG in the PTX + Huaier group was significantly lower than in the other three groups ($p < 0.05$); tumor uptakes of [^{18}F]FDG in the PTX and Huaier groups were significantly lower than the control group ($p < 0.05$).

In contrast, there was no significant difference of tumor uptake of [^{18}F]FDG in MDA-MB-231 xenografts on days 7 and 14 ($p > 0.05$, respectively; Fig. 3d). The tumor uptakes of [^{18}F]FDG in the PTX and PTX + Huaier groups were significantly lower than in the Huaier group at 21 days after treatment ($p < 0.01$, respectively; Fig. 3d). T/M ratio was significantly decreased in the Huaier group compared with the control ($p < 0.05$).

In addition, T/M ratio was remarkably correlated with the TGI on day 21 in BT474 ($r = 0.727$, $p < 0.01$; Fig. 4a) and MDA-MB-231 xenografts ($r = 0.919$, $p < 0.01$; Fig. 4b).

IHC Staining

The IHC staining results of PI3K, p-AKT, caspase-3, and VEGF in BT474 or MDA-MB-231 xenografts are demonstrated in Fig. 5a, b. The expressions of PI3K and VEGF were found with brown granular substance located mainly in

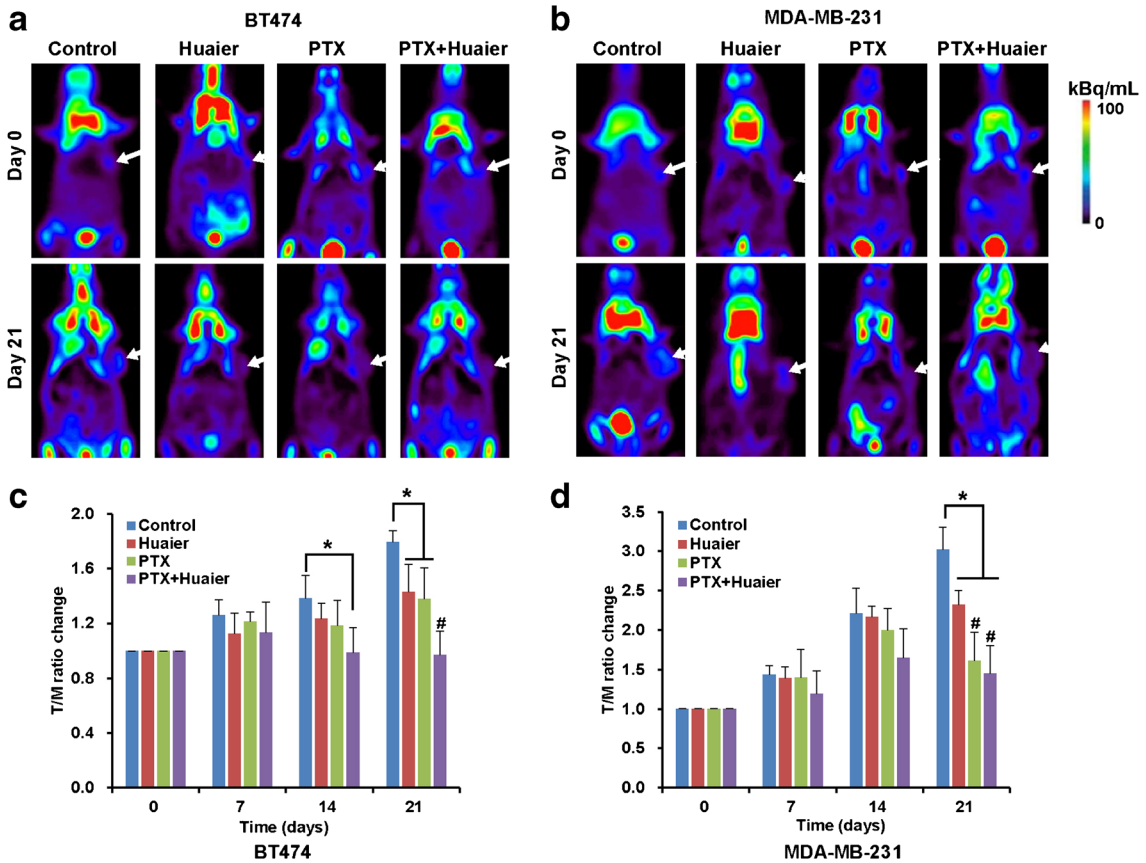

Fig. 3 *In vivo* PET imaging and [^{18}F]FDG accumulation in BT474- or MDA-MB-231-bearing mice. Typical coronal small-animal PET images of mice with **a** BT474 and **b** MDA-MB-231 xenografts implanted subcutaneously in the right flank. Small-animal PET images were acquired at day 0 (upper row) and day 21 (lower row) in all the groups. Tumors are indicated by *white arrows*. [^{18}F]FDG accumulation was measured by tumor/muscle (T/M) ratio calculated from day 0 to day 21 in **c** BT474 or **d** MDA-MB-231-bearing mice. *$p < 0.05$ *vs.* control group, #$p < 0.05$ *vs.* Huaier group.

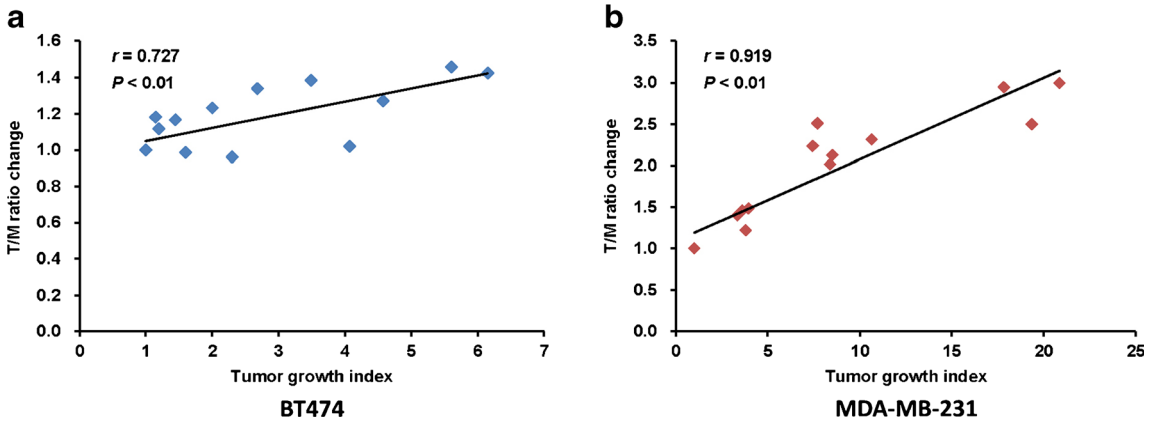

Fig. 4 The correlation between tumor/muscle (T/M) ratio and tumor growth index (TGI). T/M ratio was positively correlated with TGI on day 21 in **a** BT474- or **b** MDA-MB-231-bearing mice.

the cytoplasm, while p-AKT and caspase-3 was located in the cytoplasm and the nucleus.

For BT474 xenografts, the expression of PI3K and p-AKT in the Huaier group and PTX + Huaier group were significantly reduced relative to the PTX ($p < 0.05$; Fig. 5c) or the control group ($p < 0.01$; Fig. 5c), consistent with the tumor growth changes. However, the expression of caspase-3 presented the opposite manifestation in the Huaier ($p < 0.05$; Fig. 5c) and PTX + Huaier groups ($p < 0.05$; Fig. 5c). The PTX group and PTX + Huaier group exhibited a significant reduction of VEGF expression compared with the Huaier ($p < 0.05$; Fig. 5c) or the control group ($p < 0.05$; Fig. 5c). However, in the MDA-MB-231 xenografts, the expression of PI3K and p-AKT was moderately expressed in

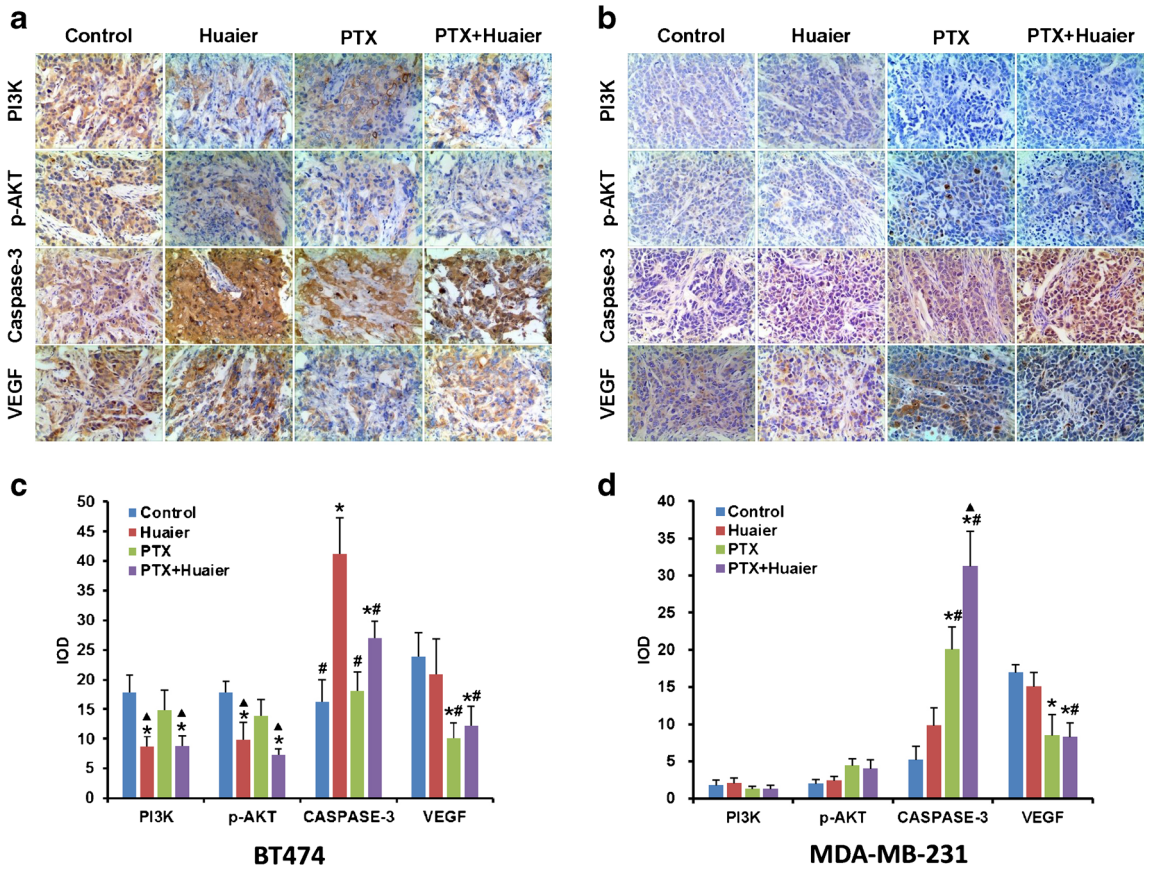

Fig. 5 IHC staining of expressions of PI3K, p-AKT, caspase-3, and VEGF in the **a** BT474 or **b** MDA-MB-231 xenografts (with magnification of ×200). The integral optical density (IOD) of expressions of PI3K, p-AKT, caspase-3, and VEGF in **c** BT474 and **d** MDA-MB-231 xenografts in the control, Huaier, PTX, and PTX + Huaier groups. *$p < 0.05$ *vs.* control group, #$p < 0.05$ *vs.* Huaier group, ▲$p < 0.05$ *vs.* PTX group.

these four groups, and no significant change was discovered after therapy ($p > 0.05$; Fig. 5d). The expression of caspase-3 significantly increased in the PTX ($p < 0.05$) and PTX + Huaier groups ($p < 0.05$) compared to Huaier or the control group. Furthermore, significant difference was found in the expression of caspase-3 between the PTX group and the PTX + Huaier group, but no significant difference was detected between the Huaier or control group ($p > 0.05$; Fig. 5d). The curvilinear trends of results in VEGF in MDA-MB-231 xenografts were consistent with that in the BT474 xenografts (Fig. 5d).

Discussion

In this study, we demonstrated promising anticancer activity of Huaier and/or PTX in BT474 and MDA-MB-231 breast cancer-bearing mice models by [^{18}F]FDG small animal PET for monitoring the dynamic glucose metabolic changes after treatment. In addition, the therapeutic effect of Huaier combined with PTX was superior to that of PTX alone in the BT474 and MDA-MB-231 xenografts.

Breast cancer is immunohistochemically divided into four molecular subtypes, mainly luminal A, luminal B, HER2 overexpression, and triple-negative subtypes. Luminal A breast cancer subtype [27] has been shown repeatedly to have a better outcome than those with the rest of subtypes across many datasets of patients with early breast cancer. Patients with HER2-enriched breast cancer seem to benefit the most from anti-HER2-targeting therapy, and those with luminal A/HER2+ subtypes seem to have a relatively better outcome compared to the other subtypes [27]. Compared with luminal A subtype, luminal B subtype has been reported to have lower expression of hormone receptors, higher expression of proliferation markers, and higher histological grade. Patients with this type of breast cancer generally present worse prognosis and a distinct profile of response to hormone therapy and chemotherapy. The triple-negative subtype has the worst treatment outcome among the four subtypes and is characterized by lack of ER, PR, and HER2 expression with the greatest aggression [28]. So far, no effective therapy has been reported for this subtype. Thus, we selected the BT474 (luminal B) and MDA-MB-231 (triple negative) breast cancer cell lines to study in the present study.

Although PTX is a major anticancer drug which has been used clinically for decades, its therapeutic effect is limited due to taxane-related toxicities [29] and drug resistance [15]. It has been reported that the mechanism of breast cancer resistance may be related to estrogen receptor (ER) co-activator dysregulation and loss of ER expression over time [30, 31]. Moreover, new evidence suggests that the PI3K/AKT/mTOR and ER signaling pathways intersect at manifold junctures and exhibit high levels of interdependence [32, 33]. Furthermore, it is suggested that inactivation of PI3K/AKT pathway in ER-positive/PTX cells can reverse PTX resistance [34]. In our study, the expressions of PI3K and p-AKT were significantly reduced in both the Huaier and PTX + Huaier groups, both of which demonstrated an effective response in BT474 (ER positive) xenografts. Therefore, we supposed that Huaier overcomes PTX's resistance to BT474 xenografts through the PI3K/AKT pathway.

Previous studies found that Huaier-induced anti-metastatic potential was triggered/sensitized by astrocyte elevated gene-1 (AEG-1) shRNA *via* inactivating the downstream PI3K/AKT pathway in the hepatocellular carcinoma and ovarian cancer [13, 35]. In the present study, the expressions of PI3K and p-AKT were significantly decreased in the Huaier and PTX + Huaier groups in BT474 xenografts. Consistent with this, the expression of caspase-3 was higher in the Huaier or PTX + Huaier group than in the other two groups, which indicated that Huaier could promote cell apoptosis in BT474 breast cancer xenograft. The expression of caspase-3 in the PTX + Huaier group was higher than in the PTX group in MDA-MB-231 xenografts, whereas the expressions of PI3K and p-AKT had no differences in the four groups. It could suggest that Huaier might enhance the inhibitory effect and induce cell apoptosis of PTX in the MDA-MB-231-bearing xenografts; however, it may not be through the PI3K/AKT pathway.

Breast cancer patients with different molecular subtypes may exhibit different therapeutic effects. As an example, patients with triple-negative breast cancers have a poorer prognosis than those with luminal breast cancer [36]. Luminal B breast cancer is ER and/or progesterone receptor (PR) positive, HER2 negative, with high Ki-67 levels or HER2 positive with any Ki-67 levels. Triple-negative breast cancer is ER, PR, and HER2 negative. Accumulated evidence has manifested that the PI3K/AKT/mTOR pathway is activated by additional nuclear ER signaling. ER promotes the transcription of several genes, including IGF-1R/insulin receptor (InsR), EGFR, which encodes the upstream factors of the PI3K/AKT/mTOR pathway [37, 38]. It is noteworthy that a gene expression signature of PI3K activation, based on cancer levels of a panel of phosphoproteins (*e.g.*, p-AKT, P-p70S6K) in ER positive tumors, was enriched in luminal B breast cancer [39]. These evidences may suggest that luminal B breast cancer has a higher PI3K activity than triple-negative breast cancer. Hence, it was observed that Huaier, which inhibits the PI3K/AKT/mTOR pathway in luminal B breast cancer, was more effective than in triple-negative breast cancer. Therefore, different molecular classifications of BT474 and MDA-MB-231 breast cancer xenografts might account for the inconsistencies of IHC results in the present study.

Moreover, oncogenes including PI3K and AKT have been found to be involved in glycolysis process [40]. In cancer cells, AKT can directly stimulate glycolytic activity, which is associated with tumor aggressiveness [41] and metabolic changes reflected in the Warburg effect [42]. Hence, the dynamic change of glucose metabolism could be used as a potential biomarker of tumor cell growth and

proliferation [43]. [^{18}F]FDG PET imaging owns an advantage over other conventional modalities in detecting glucose metabolic alterations since it can identify the biological changes of cancer in an early stage [44, 45]. Herein, we performed serial [^{18}F]FDG small animal PET imaging in BT474 and MDA-MB-231 xenografts weekly and observed different glucose metabolic trends between these two models after treatment.

In the BT474 xenografts, from day 14 onwards, accumulation of [^{18}F]FDG was significantly decreased in the PTX + Huaier group compared to the control group. Especially when the treatment period was prolonged, accumulation of [^{18}F]FDG was significantly decreased in all treatment groups as compared with the control group. Although significant consistent changes between T/M ratio and TGI were measured in tumor response studies, the T/M ratio was seen earlier than TGI in MDA-MB-231 xenografts. Interestingly, a significant difference in the volume of BT474 breast xenograft was apparent after 7 days of PTX + Huaier treatment. However, a significant decrease in tumor uptake of [^{18}F]FDG was detected only at 14 days after treatment. This difference suggests that the PTX + Huaier-mediated reduction in tumor uptake of [^{18}F]FDG is likely due to a reduction in the total number of viable tumor cells rather than decreased glucose utilization by individual cells [18]. It was also suggested that [^{18}F]FDG PET can provide earlier indications of treatment response than radiographic imaging which relies on tumor size changes in some types of malignances. Therefore, our research demonstrated that [^{18}F]FDG PET imaging could evaluate the dynamic metabolic changes in BT474 and MDA-MB-231 breast cancer xenografts in a non-invasive, real-time, and visible manner. The present research also revealed a positive correlation between PI3K/p-AKT expression and glucose metabolic changes with Huaier in BT474 xenografts. Therefore, it was noteworthy that monitoring the dynamic metabolic changes of tumor glucose utilization by [^{18}F]FDG small animal PET might indirectly reflect the status of the PI3K/AKT pathway in BT474 breast cancer xenografts.

In the present study, we suggested that Huaier might inhibit BT474 breast cancer xenograft growth through the PI3K/AKT pathway. Although Huaier combined with PTX could enhance the inhibitory effect and induce cell apoptosis in BT474 and MDA-MB-231 breast cancer xenografts, the anticancer mechanism by which Huaier exerts this effect has not yet been completely clarified; further research is still necessary to precisely define the molecular pathways.

Conclusions

[^{18}F]FDG PET imaging will be a potential method for assessing the anticancer activity of Huaier combined with PTX on BT474 and MDA-MB-231 breast cancer-bearing mice by monitoring dynamic metabolism changes. Huaier combined with PTX can significantly inhibit tumor glucose uptake in BT474 and MDA-MB-231 breast cancer xenografts. The therapeutic effect of Huaier combined with PTX in BT474 and MDA-MB-231 breast xenografts was superior to that of PTX alone.

Acknowledgments. This research was supported by grants from the National Basic Research Program of China (Grant No. 2014CB744505). We also thank Dr. Weizhong Gu for his excellent technical assistance and valuable advice on IHC staining.

Compliance with Ethical Standards. All animal studies were approved by the Zhejiang University Ethics Committee for Animal Experiments (Protocol No. ZJU201407-1-01-071).

Conflict of Interest

The authors declare that they have no conflicts of interest.

References

1. Torre LA, Bray F, Siegel RL, et l. (2015) Global cancer statistics, 2012. CA Cancer J Clin 65:87–108
2. CDC (2015) Cancer Statistics Working Group. United States cancer statistics: 1999-2012 Incidence and mortality web-based repord. Centers for Disease Control and Prevention and National Cancer Institute
3. Schneider BP, Hershman DL, Loprinzi C (2015) Symptoms: chemotherapy-induced peripheral neuropathy. Adv Exp Med Biol 862:77–87
4. Komaki K, Sano N, Tangoku A (2006) Problems in histological grading of malignancy and its clinical significance in patients with operable breast cancer. Breast Cancer 13:249–253
5. Guenancia C, Lefebvre A, Cardinale D et al (2016) Obesity as a risk factor for anthracyclines and trastuzumab cardiotoxicity in breast cancer: a systematic review and meta-analysis. J Clin Oncol 34:3157–3165
6. Morrow M (2013) Personalizing extent of breast cancer surgery according to molecular subtypes. Breast 22(Suppl 2):S106–S109
7. Borger JH, Hooning MJ, Boersma LJ et al (2007) Cardiotoxic effects of tangential breast irradiation in early breast cancer patients: the role of irradiated heart volume. Int J Radiat Oncol Biol Phys 69:1131–1138
8. Ren J, Li G, Zhao W, Lin L, Ye T (2016) Norcantharidin combined with ABT-737 for hepatocellular carcinoma: therapeutic effects and molecular mechanisms. World J Gastroenterol 22:3962–3968
9. Hu H, Luo L, Liu F et al (2016) Anti-cancer and sensibilisation effect of triptolide on human epithelial ovarian cancer. J Cancer 7:2093–2099
10. Kang Y, Hu W, Bai E et al (2016) Curcumin sensitizes human gastric cancer cells to 5-fluorouracil through inhibition of the NFkappaB survival-signaling pathway. Onco Targets Ther 9:7373–7384
11. Xiong J, Su T, Qu Z et al (2016) Triptolide has anticancer and chemosensitization effects by down-regulating Akt activation through the MDM2/REST pathway in human breast cancer. Oncotarget 7:23933–23946
12. Zhang N, Kong X, Yan S et al (2010) Huaier aqueous extract inhibits proliferation of breast cancer cells by inducing apoptosis. Cancer Sci 101:2375–2383
13. Zheng J, Li C, Wu X et al (2014) Astrocyte elevated gene-1 (AEG-1) shRNA sensitizes Huaier polysaccharide (HP)-induced anti-metastatic potency via inactivating downstream P13K/Akt pathway as well as augmenting cell-mediated immune response. Tumour Biol 35:4219–4224
14. Zheng J, Li C, Wu X et al (2014) Huaier polysaccharides suppresses hepatocarcinoma MHCC97-H cell metastasis via inactivation of EMT and AEG-1 pathway. Int J Biol Macromol 64:106–110
15. Jiang YZ, Yu KD, Peng WT et al (2014) Enriched variations in TEKT4 and breast cancer resistance to paclitaxel. Nat Commun 5:3802

16. Yang Q (2015) Neoadjuvant chemotherapy with or without Huaier granule in treating women with locally advanced breast cancer that can be removed by surgery. ClinicalTrials.gov.
17. Warburg O, Wind F, Negelein E (1927) The metabolism of tumors in the body. J Gen Physiol 8:519–530
18. McLarty K, Fasih A, Scollard DA et al (2009) ^{18}F-FDG small-animal PET/CT differentiates trastuzumab-responsive from unresponsive human breast cancer xenografts in athymic mice. J Nucl Med 50:1848–1856
19. Jacobson O, Chen X (2013) Interrogating tumor metabolism and tumor microenvironments using molecular positron emission tomography imaging. Theranostic approaches to improve therapeutics. Pharmacol Rev 65:1214–1256
20. Alberini JL, Boisgard R, Guillermet S et al (2016) Multimodal *in vivo* imaging of tumorigenesis and response to chemotherapy in a transgenic mouse model of mammary cancer. Mol Imaging Biol 18:617–626
21. Schlaepfer IR, Glode LM, Hitz CA et al (2015) Inhibition of lipid oxidation increases glucose metabolism and enhances 2-deoxy-2-[(18)F]Fluoro-D-glucose uptake in prostate cancer mouse xenografts. Mol Imaging Biol 17:529–538
22. Campbell MJ, Hamilton B, Shoemaker M et al (2002) Antiproliferative activity of Chinese medicinal herbs on breast cancer cells *in vitro*. Anticancer Res 22:3843–3852
23. Powell CB, Fung P, Jackson J et al (2003) Aqueous extract of herba Scutellaria barbatae, a chinese herb used for ovarian cancer, induces apoptosis of ovarian cancer cell lines. Gynecol Oncol 91:332–340
24. Pasquier E, Ciccolini J, Carre M et al (2011) Propranolol potentiates the anti-angiogenic effects and anti-tumor efficacy of chemotherapy agents: implication in breast cancer treatment. Oncotarget 2:797–809
25. Shah C, Miller TW, Wyatt SK et al (2009) Imaging biomarkers predict response to anti-HER2 (ErbB2) therapy in preclinical models of breast cancer. Clin Cancer Res 15:4712–4721
26. Zhang H, Song F, Xu C et al (2015) Spatiotemporal PET imaging of dynamic metabolic changes after therapeutic approaches of induced pluripotent stem cells, neuronal stem cells, and a Chinese patent medicine in stroke. J Nucl Med 56:1774–1779
27. Prat A, Pineda E, Adamo B et al (2015) Clinical implications of the intrinsic molecular subtypes of breast cancer. Breast 24(Suppl 2):S26–S35
28. Palma G, Frasci G, Chirico A et al (2015) Triple negative breast cancer: looking for the missing link between biology and treatments. Oncotarget 6:26560–26574
29. Boso V, Herrero MJ, Santaballa A et al (2014) SNPs and taxane toxicity in breast cancer patients. Pharmacogenomics 15:1845–1858
30. Gutierrez MC, Detre S, Johnston S et al (2005) Molecular changes in tamoxifen-resistant breast cancer: relationship between estrogen receptor, HER-2, and p38 mitogen-activated protein kinase. J Clin Oncol 23:2469–2476
31. Osborne CK, Schiff R (2011) Mechanisms of endocrine resistance in breast cancer. Annu Rev Med 62:233–247
32. Simoncini T, Hafezi-Moghadam A, Brazil DP et al (2000) Interaction of oestrogen receptor with the regulatory subunit of phosphatidylinositol-3-OH kinase. Nature 407:538–541
33. Campbell RA, Bhat-Nakshatri P, Patel NM et al (2001) Phosphatidylinositol 3-kinase/AKT-mediated activation of estrogen receptor alpha: a new model for anti-estrogen resistance. J Biol Chem 276:9817–9824
34. Cai J, Chen S, Zhang W et al (2014) Salvianolic acid A reverses paclitaxel resistance in human breast cancer MCF-7 cells via targeting the expression of transgelin 2 and attenuating PI3 K/Akt pathway. Phytomedicine 21:1725–1732
35. Yan X, Lyu T, Jia N et al (2013) Huaier aqueous extract inhibits ovarian cancer cell motility via the AKT/GSK3beta/beta-catenin pathway. PLoS One 8:e63731
36. Korsching E, Jeffrey SS, Meinerz W et al (2008) Basal carcinoma of the breast revisited: an old entity with new interpretations. J Clin Pathol 61:553–560
37. Miller TW, Perez-Torres M, Narasanna A et al (2009) Loss of phosphatase and Tensin homologue deleted on chromosome 10 engages ErbB3 and insulin-like growth factor-I receptor signaling to promote antiestrogen resistance in breast cancer. Cancer Res 69:4192–4201
38. Miller TW, Rexer BN, Garrett JT, Arteaga CL (2011) Mutations in the phosphatidylinositol 3-kinase pathway: role in tumor progression and therapeutic implications in breast cancer. Breast Cancer Res 13:224
39. Creighton CJ, Fu X, Hennessy BT et al (2010) Proteomic and transcriptomic profiling reveals a link between the PI3K pathway and lower estrogen-receptor (ER) levels and activity in ER+ breast cancer. Breast Cancer Res 12:R40
40. Iurlaro R, Leon-Annicchiarico CL, Munoz-Pinedo C (2014) Regulation of cancer metabolism by oncogenes and tumor suppressors. Methods Enzymol 542:59–80
41. Elstrom RL, Bauer DE, Buzzai M et al (2004) Akt stimulates aerobic glycolysis in cancer cells. Cancer Res 64:3892–3899
42. Robey RB, Hay N (2009) Is Akt the "Warburg kinase"?—Akt-energy metabolism interactions and oncogenesis. Semin Cancer Biol 19:25–31
43. Lemons JM, Feng XJ, Bennett BD et al (2010) Quiescent fibroblasts exhibit high metabolic activity. PLoS Biol 8:e1000514
44. Phelps ME (2000) Positron emission tomography provides molecular imaging of biological processes. Proc Natl Acad Sci U S A 97:9226–9233
45. Gambhir SS (2002) Molecular imaging of cancer with positron emission tomography. Nat Rev Cancer 2:683–693